Results in Physics 19 (2020) 103496

Contents lists available at ScienceDirect

Results in Physics

journal homepage: www.elsevier.com/locate/rinp

The influence of heavy elements on the ionizing radiation shielding efficiency and elastic properties of some tellurite glasses: Theoretical investigation

A.M.A. Mostafa [a,b], Shams A.M. Issa [b,c], Hesham M.H. Zakaly [b,d,*], M.H.M. Zaid [e,*], H.O. Tekin [f], K.A. Matori [e], H.A.A. Sidek [e], Reda Elsaman [b]

[a] Physics Department, College of Science, Jouf University, P.O. Box: 2014, Sakaka, Saudi Arabia
[b] Physics Department, Faculty of Science, Al-Azhar University, 71524 Assuit, Egypt
[c] Physics Department, Faculty of Science, University of Tabuk, Tabuk, Saudi Arabia
[d] Institute of Physics and Technology, Ural Federal University, Ekaterinburg, Russia
[e] Department of Physics, Universiti Putra Malaysia, 43400 Serdang, Selangor, Malaysia
[f] Medical Diagnostic Imaging Department, College of Health Sciences, University of Sharjah, Sharjah 27272, United Arab Emirates

ARTICLE INFO

Keywords:
Tellurite glasses
Mechanical properties
Nuclear shielding properties
FLUKA code

ABSTRACT

The impact of adding PbO and WO_3 on the mechanical properties and radiation shielding efficiency of 4 different glass samples labeled as TWP1, TWP2, TWP3, and TWP4 (samples codes) was studied via the Makishima and Mackenzie model (MMD), Rocherulle model (RD), XCOM database, FLUKA code, and Phys-X/PSD software. According to MMD, Young's (Y), bulk (K), shear (G) modulus values increase from 59.13 to 62.80 GPa, from 37.76 to 43.86 GPa, from 25.48 to 26.55 GPa, and from 71.73 to 79.26 GPa for TWP1 and TWP4 glasses, respectively. 277.833, 358.768, 465.048 and 570.786 cm^{-1} values are the highest linear attenuation coefficient (μ) values for TWP1, TWP2, TWP3 and TWP4 glasses at 0.015 MeV. The results refer that the TWP4 glass sample has the highest radiation shielding and mechanical properties. The results indicated that the addition of lead and tungsten to the investigated samples improves their elastic and radiation shielding properties. Thus, the TWP4 sample is the best compared to the other glass samples.

Introduction

The continued development in various fabrications and technologies requests the utilization of more ionizing radiations. The ionizing radiations have considerable significance due to their substantial applications in different fields such as accelerator [1], medical treatment [2], space [3], factory [4], and agriculture [5]. The staffs working in the fields that use radiation sources are every day exposed to various kinds of ionizing radiation and besides confrontation large hazards to their life [6]. Among nuclear radiations, gamma has high penetration power in materials due to their zero mass and charge. Thus, the exposure for a long time of gamma may be a reason to damage the cellular and genetic structure which causes cancer and death [7,8]. For the protection from hurtful radiation exposures, many investigators have fabricated different types of shielding materials [9–11]. One of these materials is concrete which is used to protect the staff from hurtful exposure to radiation. Unfortunately, the concretes have some disadvantages such as opacity and immovability. Thus, nowadays the concretes are not preferred and have been changed by other useful materials [12,13].

Radiological safety is depending on the ability of a material to decrease the number of photons and their energy when exposed to radiation. For this objective, perfect shielding glasses for radiations have been fabricated by researchers [14–16]. Due to the lightweight, low cost, easy preparation, easy movement, transparency, and high mechanical power of glass materials, they have been considerably used in radiation shielding. Many fabricated materials such as Te, Si, V, Pb, W, and Bi glasses have been used as shielding materials [17–19]. Tellurite glass is known as the preferred materials for various technology applications due to their perfect physical properties like high refractive index, good chemical resistance, low crystallization ability, and low melting point [20]. Because the Pb reinforces the devitrification resistance and has a low melting point, it considers as unique in its impact on the glass

* Corresponding authors at: Institute of Physics and Technology, Ural Federal University, Ekaterinburg, Russia (H.M.H. Zakaly).
E-mail addresses: h.m.zakaly@azhar.edu.eg (H.M.H. Zakaly), mhmzaid@upm.edu.my (M.H.M. Zaid).

https://doi.org/10.1016/j.rinp.2020.103496
Received 19 August 2020; Received in revised form 29 September 2020; Accepted 9 October 2020
Available online 15 October 2020

Table 1
Chemical composition (mol%) and elements (wt. %) and density for glasses.

Code	TeO_2	WO_3	PbO	O	Te	W	Pb	ρ (g/cm^3)
TWP1	90	10	0	0.2011	0.7196	0.0793	–	5.798
TWP2	75	15	10	0.1886	0.5996	0.1189	0.0928	6.221
TWP3	50	30	20	0.1767	0.4797	0.2379	0.0928	6.831
TWP4	40	40	20	0.1773	0.3198	0.3172	0.1857	7.018

structure. Furthermore, it plays a double role in glasses; one as a modifier and other as glass former [21]. Moreover, the addition of both WO_3 and PbO improves the shielding properties of the studied glasses. Al-Hadeethi and Sayyed reported that the mass attenuation coefficient (μ_m) reduces with an increase in the energy whereas it increases when TeO_2 is replaced by PbO [22]. Alalawi et al. studied the Influence of lead and zinc oxides on the radiation shielding properties of tellurite glass systems. They found that the addition of PbO changed the gamma and neutron properties of the PbO-TeO_2 glasses [23].

Oxide glasses containing TeO_2 as the main component have extreme optical properties, for example, $n = 2.1–2.3$. Besides, they have adequate light transmittance in the visible and infrared regions, up to about 7 μm. For this reason, tellurite glasses are essential for the design of scientific instruments and have therefore been the subject of extensive study. Pure TeO_2 metals, do not harden to Glass. Whenever glass formation has been reported in the literature, contamination of the ceramic Crucible has generally resulted in the formation of multicomponent Glass [24]. As early as 1834, Berzelius [25] recognized that TeO_2 could form Glass with various metal oxides, especially BaO. From 1952, from the works of Stanworth [26,27], systematic studies were conducted by various authors [28].

Classical dielectric theory gives a series of relationships between the refractive index and the density of solids. It is generally accepted that the refractive index n and density ρ of many conventional glasses can be changed by changing the composition of the base glass[28], changing the sample temperature [29], assigning the sample to pressure, and inducing a new history of the transformation range, such as repeated annealing [30,31]. The objective of this work is to obtain the attenuation efficiency of WO_3 and PbO based TeO_2 glasses via the NISTXCOM database, FLUKA code, and Phy-X/PSD software in the energy from 0.015 to 15 MeV. We will also study the elastic modulus of the investigated glasses to use as radiation shielding.

Materials and methods

Four glass samples of TeO_2–WO_3–PbO glasses have been taken from reference [32]. The detailed label, chemical compositions, and densities have been listed in Table 1. For all related equations along with explicit routine interpretations for linear attenuation coefficient, mass attenuation coefficient, Have value layer, Mean free path, effective atomic number, energy absorption buildup factors, Electronic cross-section, Atomic cross-section, Effective conductivity, and Effective removal cross-sections for fast neutrons [μ, μ_m, HVL, MFP, Z_{eff}, EABF, ECS, ACS, C_{eff}, and Σ_R] respectively, are suggested to take a glance at references [33–43]. After that, for the descriptions on the employed XCOM [44], Phy-X/PSD software [45] and details on the FLUKA (http://www.fluka.org) code [46–48]. FLUKA [49,50] is a Monte Carlo simulation package for different models of particle transport and interaction with matter. FLUKA can model the interaction and propagation of>60 different particles in a matter-such as heavy ions, electrons, neutrons, photons, neutrinos, and muons-in many research areas: shielding design, detector response study, cosmic ray study, medical physics, and dosimetry calculations[51]. The use of this method requires knowledge of the chemical or elemental composition and density of the material, as well as its input physical characteristics to perform these calculations [6,47,52].

In the present simulation, we attempted to estimate the mass attenuation coefficients of glass samples for photons with energies $0.015*10^{+3}$ to $15*10^{+3}$ keV using Fluka Monte Carlo code because of its event-by-Event Tracking feature. the BEAMPOS map was used to determine the position and direction of a radioactive source, considered as a beam of unidirectional monoenergetic photons (0.2 cm) along the Z-axis with different energies. Then the angular and energy distribution of the source, as well as the type of particle and its energy, were known on the beam map. For low-energy photon transport, the energy cutoff is 10^{-6} GeV on the EMFCUT board. The photons were recorded with the Nai (Tl) Scintillation detector (7.62 × 7.62 cm). The detector was placed inside a collimator lead cylinder having an outer and inner diameter of 12 and 0.2 cm, respectively, at a length of 15 cm.la Zone NaI was implemented as a track length Fluence estimator using the USRTRACK dashboard. In geometry, the sample was placed between the source and the detector surface.

The material map describing the selected sample contains the mixture name, mass fraction, density, etc. and is used with the desired Composite maps to determine the exact composition of the sample. The modeling processes are performed between 106 and 206 number of primary photons to obtain a statistical error less than 1%. The Fluence of the photon in the detector volume was evaluated using a usrbin card. The sample was simulated as a 2 cm diameter cylinder with variable thicknesses ranging from 0.2 to 0.5 cm. (Fig. 1). The mechanical properties of the studied glasses have been calculated using Makishima and Mackenzie (MMD) and Rocherulle (BD) models [53–55]

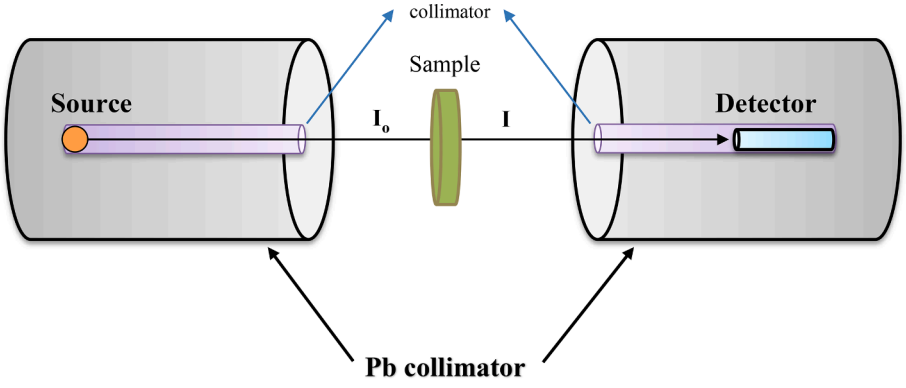

Fig. 1. FLUKA Monte Carlo simulation setup used for mass attenuation coefficients calculations of glasses.

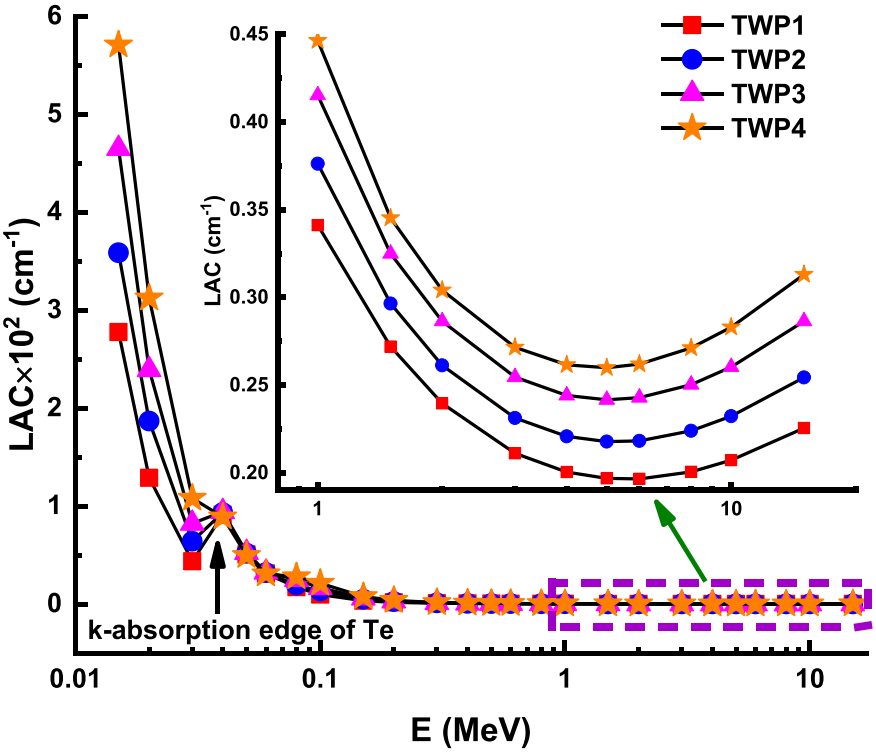

Fig. 2. Variation of linear attenuation coefficient (LAC) with photon energy for all glasses.

Results and discussion

Shielding parameters

The μ is an advantageous parameter to evaluate the attenuation shielding efficiency of glass material against gamma radiations. Among investigated glasses, TWP4 glass has the highest μ value which is 570.786 cm^{-1} at 0.015 MeV but with an increase in energy, μ value reduces to be 0.313 cm^{-1} at 15 MeV. The accountable factors of this reduce are PE (photoelectric effect), CS (Compton scattering), and PP (pair production) processes at low, medium, and high energy, respectively, which depicts the changes of μ with glass composition and energy as specified in Fig. 2 [14,36,45]. Density has an essential role to reinforce the μ values of glasses. This behavior is due to the replacement of the higher molecular weight of WO_3 and PbO with the lower molecular weight TeO_2.

The μ_m values of all glasses are drawn in Fig. 3 (a-d). As published in the literature, the μ_m for TWP1, TWP2, TWP3, and TWP4 glasses has the same behavior at low and high energy. The μ_m values are 47.919, 57.670, 68.079 and 81.332 cm^2/g at 0.015 MeV and are 0.039, 0.041, 0.042 and 0.045 cm^2/g at 15 MeV for TWP1, TWP2, TWP3 and TWP4 glasses, respectively. The increment μ_m value from sample TWP1 to TWP4 elucidates that μ_m values are dependent on the WO_3 and PbO contents. In the selected photon energy (0.015–15 MeV), at the beginning (0.015 to 0.05 MeV), μ_m decreases quickly then decreases slowly and at high energy stayed unchanged. This due to the dominations of PE, CS, and PP processes. It is observed that the TWP4 sample has great μ_m value as compared to other glass samples that conclude the predominant impact of WO_3 and PbO concentration. Fig. 3 (a-d) shows μ_m values comparison obtained using NISTXCOM, FLUKA code, and Phy-X/PSD, correspondingly. It is worth mentioning that some very small deviations in μ_m values deduced by computational and theoretical methods could commonly take place due to slight variations in considered mathematical and physical models, geometry, and ambiguities in the atomic data, etc. for each method. The Relative differences (RD) between XCOM and both Phys-X/PSD and FLUKA code for all glasses ranged approximately from −4 to 4% (Fig. 4 (a-b). For example, at 1.5 MeV, 0.04841, 0.04920 and 0.04831 cm^2/g are the μ_m values achieved for TWP4 glass using NISTXCOM [51], Phy-X/PSD, and FLUKA code, respectively.

Electronic cross-section (ECS) and Atomic cross-section (ACS) are listed in Table 2 and Table 3. The ECS and ACS values changed with the energy and both WO_3 and PbO contents in the glasses. With increasing, gamma energy, TWP1, TWP2, TWP3, and TWP4 samples' ECS and ACS exhibit the same trend in variations. As the ρ of glasses increase from 5.798 to 7.018 g/cm^3, ECS and ACS values appropriately improved, for example, via Phy-X/PSD software, at 0.03 MeV, the calculated respective ECS and ACS for TWP1, TWP2, TWP3, and TWP4 samples are 4.77×10^{-25}, 5.13×10^{-25}, 5.43×10^{-25}, and 5.84×10^{-25} cm^2/g and 1.50×10^{-23}, 1.86×10^{-23}, 2.15×10^{-23} and 2.56×10^{-23} cm^2/g, respectively. With increasing gamma energy results detect that photons can largely go through the glass, requiring appropriate thickness to further decrease them. As mentioned for μ and μ_m values for all glasses, the ECS and ACS values depending on photon energy and PE, CS, and PP processes dominate at low, medium, and high energy, respectively. TWP4 glass comparatively has higher ECS and ACS in all studded samples within the selected photon energy range, suggesting it as a prime γ-ray absorber.

MFP is the most considerable factor that immediately explains the capacity of any barrier to decrease the gamma radiations. Therefore, the glass with lower MFP has good shielding competence. The obtained values indicate that the MFP of glasses increases with photon energy (Fig. 5) which signifies that at higher energy, large numbers of photons can penetrate through the glasses. Also obvious from Fig. 5 that the value of MFP reduces significantly with increasing the WO_3 and PbO

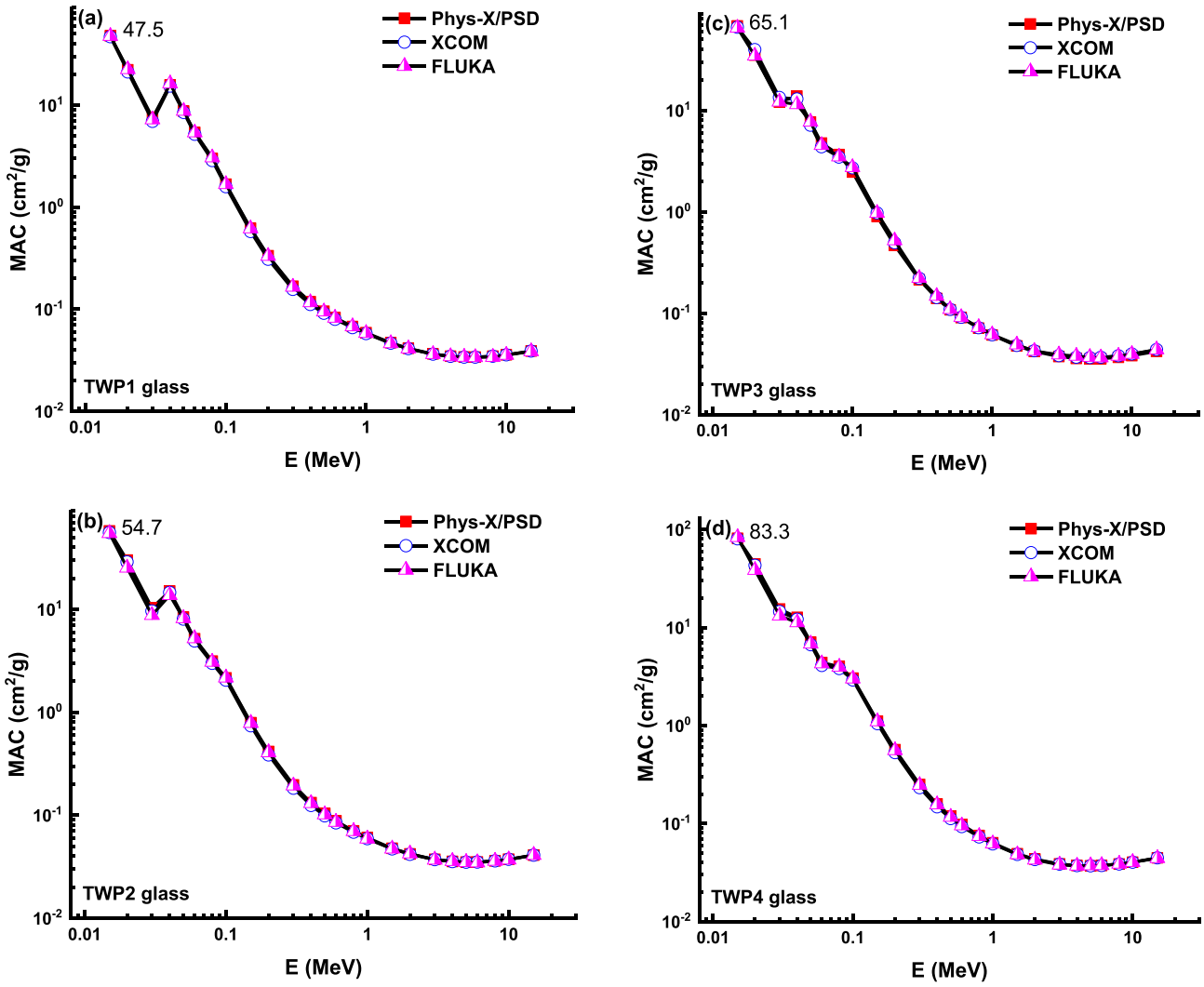

Fig. 3. (a-d) Comparison of XCOM, Phys-X/PSD and FLUKA codes computed mass attenuation coefficients (MAC) versus photon energy for all glasses.

contents. The density of the glasses also influences the MFP; highest density, lowest MFP. HVL is capable to provide persuasive information in connection with the shielding ability of samples as it appropriates the desired thickness to decrease the number of photons to half of its original. Fig. 6 represents the HVL for the TWP1, TWP2, TWP3, and TWP4 glasses. It is obvious from Fig. 6 that on raising the contents of W and Pb, the HVL declines. Sample TWP4 that has the highest concentration (W and Pb) and density, indicates that it is the best absorption among all the studied samples. Fig. 7 represents the HVL values of TWP4 sample comparison with RS253G18, RS360, and RS520 (SCHOTT) commercially existing nuclear radiation shielding glasses [56]. Also, Fig. 8 represents the HVL values of TWP4 sample comparison with OC (Ordinary), BM (Basalt–magnetite), HS (Hematite–serpentine), and SSC (Steel-scrap) concrete [57]. At compared three 0.2, 0.662, and 1.25 MeV, the TWP4 sample has the lowest HVL value than those of commercial RS253G18, RS360, and RS520 glasses (Fig. 7). Furthermore, within 0.015–15 MeV photon energy range, in comparison to all types of concretes HVL, TWP4 has the lowest values (Fig. 8). These results refer that as TWP4 contains higher MAC than the compared materials, it has a better gamma shielding efficiency over commercial glasses and concretes.

Another essential factor also an assistant to discover the attenuation capability of glass is the effective atomic number (Z_{eff}). Addition the heavy metals oxides to glass materials are important to increment the Z_{eff}. As mentioned in many investigations, the glass material with high Z_{eff} has excellent radiation protection prospects [58]. For TWP1, TWP2, TWP3, and TWP4 glasses, Z_{eff} values within 0.015–15 MeV photon energy range are presented in Fig. 9. Z_{eff} values for all glasses, larger values in the lowest energy region where PE predominates, while minimal quantities transpire at medium energy range due to CS command and minor increments take place at higher energies because of PP phenomenon influence. As shown in Fig. 9 the TWP1 glass ($90TeO_2$-$10WO_3$) has the lowest Z_{eff} values while the TWP4 glass ($40TeO_2$-$40WO_3$-20PbO) has the highest Z_{eff} values within selected photon energy. The correlation between Z_{eff} and effective electron density (N_{eff}) and Effective conductivity (C_{eff}) are shown and listed in Fig. 10 and Table 4, respectively. The photons penetrating the glass collision the electrons and convert them into free electrons. The changes in the number of free electrons lead to a change in the electrical conductivity of the material. The glass that electrical conductivity changes according to the density of photon and energy could change the shielding features. Thus, it is very substantial to know the C_{eff} factor, which displays how a glass preserves its features according to nuclear applications. As observed in Fig. 10 and Table 4, N_{eff} and C_{eff} behaviors are identical to Z_{eff} behavior.

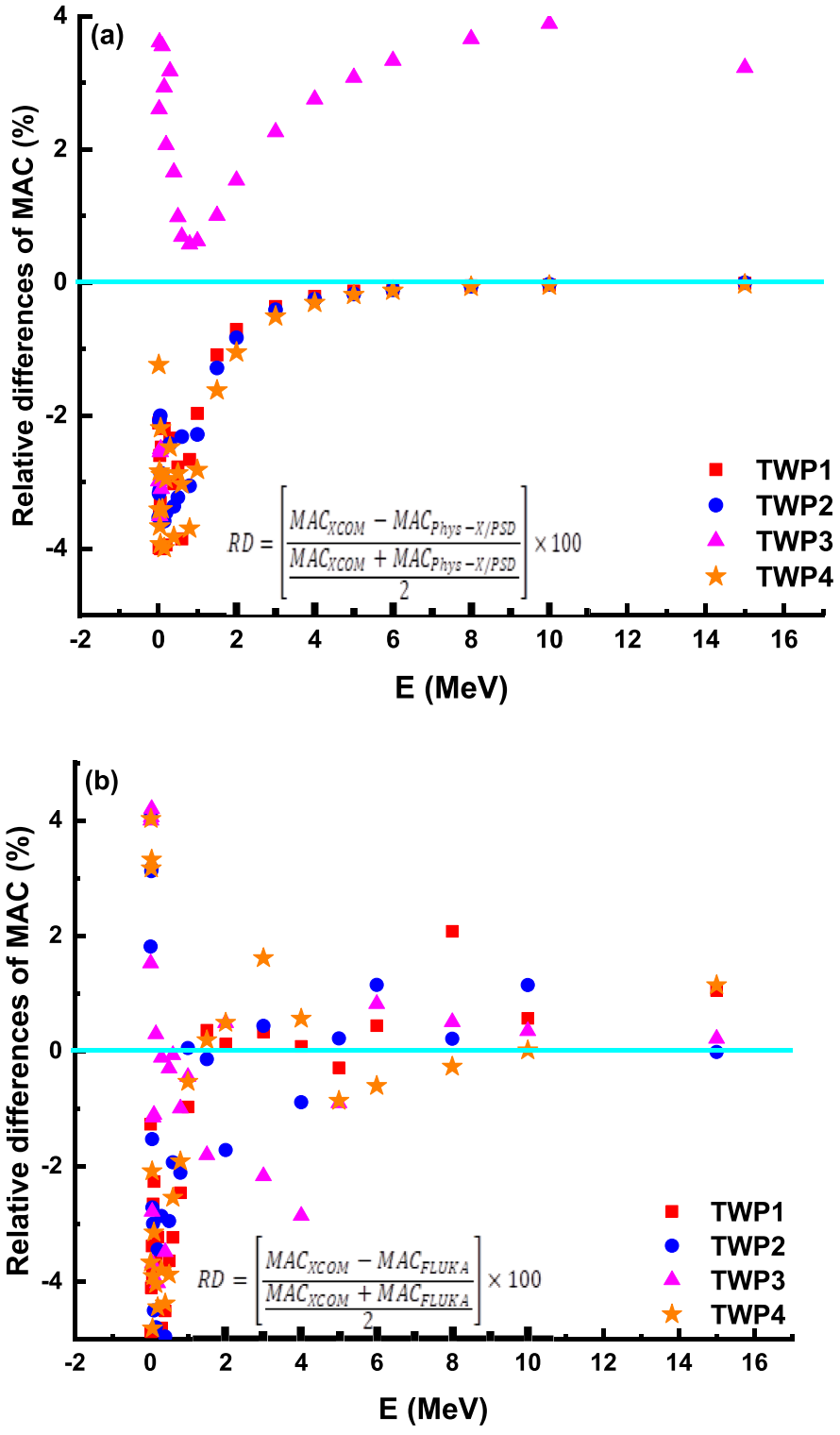

Fig. 4. (a-b) Relative differences (RD) between XCOM and (a) Phys-X/PSD (b) FLUKA code for all glasses.

Table 2
Electronic cross section (ECS) (cm^2/g) for glass samples.

E (MeV)	TWP1	TWP2	TWP3	TWP4
1.50E−02	8.00E−23	9.24E−23	1.09E−22	1.23E−22
2.00E−02	3.71E−23	4.66E−23	5.46E−23	6.56E−23
3.00E−02	1.27E−23	1.61E−23	1.89E−23	2.28E−23
4.00E−02	2.70E−23	2.62E−23	2.48E−23	2.16E−23
5.00E−02	1.52E−23	1.47E−23	1.39E−23	1.22E−23
6.00E−02	9.46E−24	9.19E−24	8.71E−24	7.66E−24
8.00E−02	5.13E−24	5.36E−24	6.18E−24	6.42E−24
1.00E−01	2.99E−24	3.57E−24	4.07E−24	4.72E−24
1.50E−01	1.26E−24	1.47E−24	1.64E−24	1.88E−24
2.00E−01	7.74E−25	8.75E−25	9.58E−25	1.07E−24
3.00E−01	4.77E−25	5.13E−25	5.43E−25	5.84E−25
4.00E−01	3.76E−25	3.94E−25	4.08E−25	4.29E−25
5.00E−01	3.24E−25	3.34E−25	3.43E−25	3.55E−25
6.00E−01	2.90E−25	2.97E−25	3.03E−25	3.11E−25
8.00E−01	2.47E−25	2.51E−25	2.54E−25	2.58E−25
1.00E+00	2.19E−25	2.21E−25	2.23E−25	2.26E−25
1.50E+00	1.77E−25	1.78E−25	1.79E−25	1.80E−25
2.00E+00	1.54E−25	1.55E−25	1.56E−25	1.57E−25
3.00E+00	1.29E−25	1.30E−25	1.31E−25	1.32E−25
4.00E+00	1.16E−25	1.18E−25	1.19E−25	1.20E−25
5.00E+00	1.09E−25	1.11E−25	1.12E−25	1.13E−25
6.00E+00	1.05E−25	1.06E−25	1.08E−25	1.09E−25
8.00E+00	1.00E−25	1.02E−25	1.04E−25	1.05E−25
1.00E+01	9.89E−26	1.01E−25	1.03E−25	1.04E−25
1.50E+01	9.98E−26	1.02E−25	1.05E−25	1.06E−25

Table 3
Atomic cross section (ACS) (cm^2/g) for glass samples.

E (MeV)	TWP1	TWP2	TWP3	TWP4
1.50E−02	4.27E−21	5.45E−21	6.83E−21	8.33E−21
2.00E−02	1.98E−21	2.84E−21	3.52E−21	4.56E−21
3.00E−02	6.72E−22	9.74E−22	1.21E−21	1.58E−21
4.00E−02	1.40E−21	1.42E−21	1.39E−21	1.30E−21
5.00E−02	7.80E−22	7.90E−22	7.72E−22	7.25E−22
6.00E−02	4.81E−22	4.88E−22	4.78E−22	4.50E−22
8.00E−02	2.67E−22	2.96E−22	3.69E−22	4.09E−22
1.00E−01	1.50E−22	2.03E−22	2.47E−22	3.11E−22
1.50E−01	5.52E−23	7.46E−23	9.02E−23	1.13E−22
2.00E−01	2.97E−23	3.92E−23	4.67E−23	5.80E−23
3.00E−01	1.50E−23	1.86E−23	2.15E−23	2.56E−23
4.00E−01	1.05E−23	1.25E−23	1.41E−23	1.62E−23
5.00E−01	8.52E−24	9.80E−24	1.08E−23	1.22E−23
6.00E−01	7.36E−24	8.30E−24	9.07E−24	1.00E−23
8.00E−01	6.03E−24	6.65E−24	7.16E−24	7.74E−24
1.00E+00	5.24E−24	5.71E−24	6.10E−24	6.51E−24
1.50E+00	4.18E−24	4.50E−24	4.78E−24	5.04E−24
2.00E+00	3.68E−24	3.97E−24	4.21E−24	4.44E−24
3.00E+00	3.24E−24	3.51E−24	3.74E−24	3.96E−24
4.00E+00	3.08E−24	3.35E−24	3.59E−24	3.82E−24
5.00E+00	3.03E−24	3.31E−24	3.55E−24	3.79E−24
6.00E+00	3.02E−24	3.31E−24	3.57E−24	3.82E−24
8.00E+00	3.08E−24	3.40E−24	3.68E−24	3.96E−24
1.00E+01	3.18E−24	3.53E−24	3.83E−24	4.13E−24
1.50E+01	3.46E−24	3.86E−24	4.21E−24	4.57E−24

Fig. 11 (a-d) and Fig. 12 (a-d) describe the changing of EBF and EABF against photon energy up to 40 mfp for TWP1, TWP2, TWP3, and TWP4 glasses. Corresponding to this, within the gamma energy range of 0.015–15 MeV, for all selected glasses, Table 5 (a-d) presents the estimated Z_{eq} and associated G-P fitting parameters for EBF and EABF assessments. The trend of the buildup factors with energy is similar for all glasses. EABF and EBF were low at energies less than 100 keV and increase steadily with increasing energy up to 1 MeV before and then descending as the energy rises. The lower EABF and EBF at low and high energies are due to PE and PP processes. However, in the region around 1 MeV, the CS dominates the photon interaction processes. However, at larger penetration depths (>10 mfp) and greater energies (>6 MeV), EBF and EABF values increased noticeably due to the occurrence of persistent secondary photons scatterings. These allow for increased photons buildup in glasses. Besides, for TWP1, TWP2, TWP3, and TWP4 glasses, EBF and EABF values increased gradually with the increasing penetration depth from 0.5 to 40 mfp as scattering volume improves. Here, EBF and EABF present a behavior against the incident gamma energy and penetration depth for each glass. For all studied glasses, the calculated EBF and EABF values decrease with the replacement of WO_3 and PbO by TeO_2 content, and accordingly, the lowest values are achieved for the TWP4 sample as it contains higher Z_{eq} and Z_{eff} values, suggesting it as a great shield for gamma.

It is widely known that neutrons exhibit greater radiobiological outcomes compared to photons, necessitating adequate attenuator of them for radiation workers' safety. Fundamentally, by scattering and absorption processes, neutron shielding is realized. For TWP1, TWP2, TWP3, and TWP4 glasses, in Fig. 13 we provided the Σ_R estimation procedures and the related Σ_R values. Here, the derived Σ_R for TWP1, TWP2, TWP3 and TWP4 samples are 0.108, 0.112, 0.117, and 0.119 cm^{-1}, respectively. It means that the Σ_R values increase with increasing WO_3 and PbO concentration, which indicates that the heavy elements W and Pb also supports Σ_R. Table 6 observes that the TWP4 sample has the bigger Σ_R value compared to corresponding Graphite, Water [59], OC, HSC, Ilmenite-limonite concrete, Basalt-magnetite concrete, Ilmenite concrete, [57], VPZn8 glass [60], C20 glass [61], TBBT30 glass [62], S2 ceramic [63], 95TeLi glass [64] and Polyamide polymer [65].

For TWP1, TWP2, TWP3, and TWP4 samples, Fig. 14, Fig. 15, and Fig. 16 explain the evaluated Ψ_{proton}, Ψ_{Alpha}, and $\Psi_{Electron}$ variations within the kinetic energy (KE) range of 0.015–15 MeV, respectively. From Fig. 14 and Fig. 15, with KE, both Ψ_{proton}, Ψ_{Alpha} values have the same behaviors. With increasing KE from 15 KeV, both Ψ_{proton}, Ψ_{Alpha} rise sharply, reaching the maximum values at 0.09 MeV and 0.7 MeV, respectively. With further KE enhancement, Ψ_{proton}, Ψ_{Alpha} values both decreased progressively. Furthermore, the TWP4 sample has the lowest values among all the studied samples. Fig. 16 shows, within 0.015–15 MeV, the calculated $\Psi_{Electron}$ values change while the inset plot exhibits enlarged 0.015–0.05 and 10–15 MeV. For all glasses, the $\Psi_{Electron}$ values are the lowest up to 1 MeV. In general, the electrons can be excellently stood by TWP4 sample (up to 1 MeV) compared to the other glasses

Mechanical properties

The rigidity of a glass shield could be described in terms of the mechanical properties. Based on the dissociation energy per unit volume (G_t), packing density (V_t and C_t), and chemical composition, Makishima and Mackenzie (MMD), and Rocherulle (BD) were suggested the theoretical models calculate the elastic moduli as following [53–55]. For all related equations along with explicit routine interpretations for elastic modulus are suggested to take a glance at references [66,67]. Where, Y, K, G, L, and σ are the Young's, bulk, shear, longitudinal moduli, and Poisson's ratio. The Y, K, G, L, and σ values according to MMD and RD are listed in Table 7 and Table 8, respectively. σ is an important parameter to explain the rigidity of glasses, where it depends on glass composition. Moreover, σ determines the dimension and crosslink density of the glasses. σ has values ranged from 0.1 to 0.2 and from 0.3 to 0.5 for high cross density and low crosslink density, respectively [68]. The values of σ are ranged from 0.24 to 0.26 for investigated glass samples (Table 7). This indicates that these glasses approach towards the high cross-link density network and high rigidity. The effect of WO_3 and PbO on the rigidity of glasses is observed also from the increasing value of elastic constants (Y, K, G, L) according to both MMD and RD. The values of elastic moduli are increasing with increasing WO_3 and PbO,

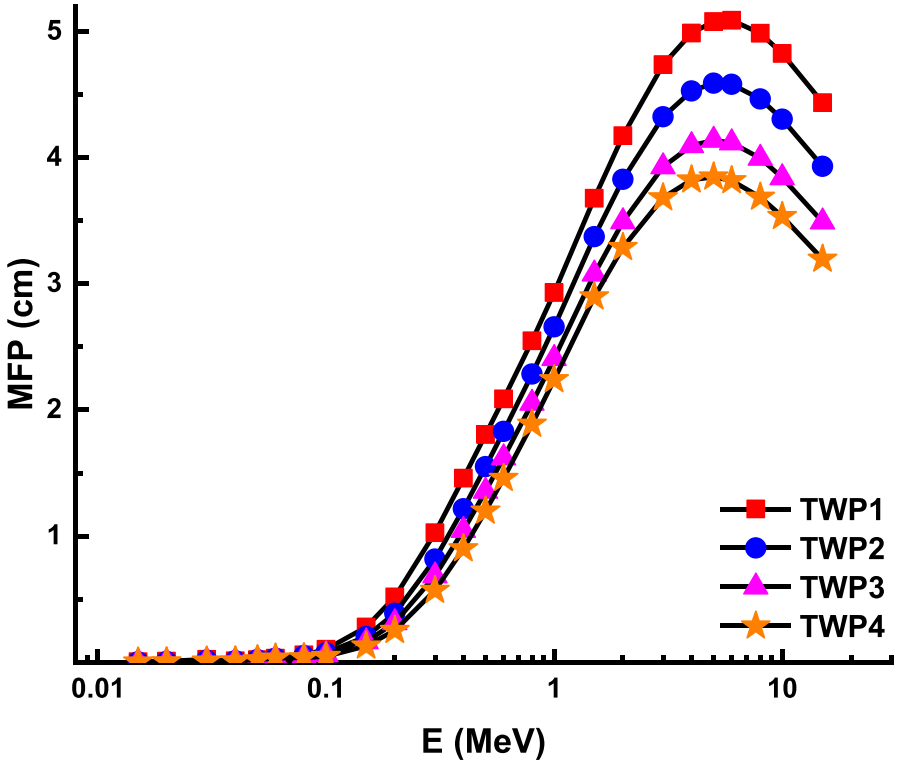

Fig. 5. Variations of mean free path (MFP) with photon energy for all glasses.

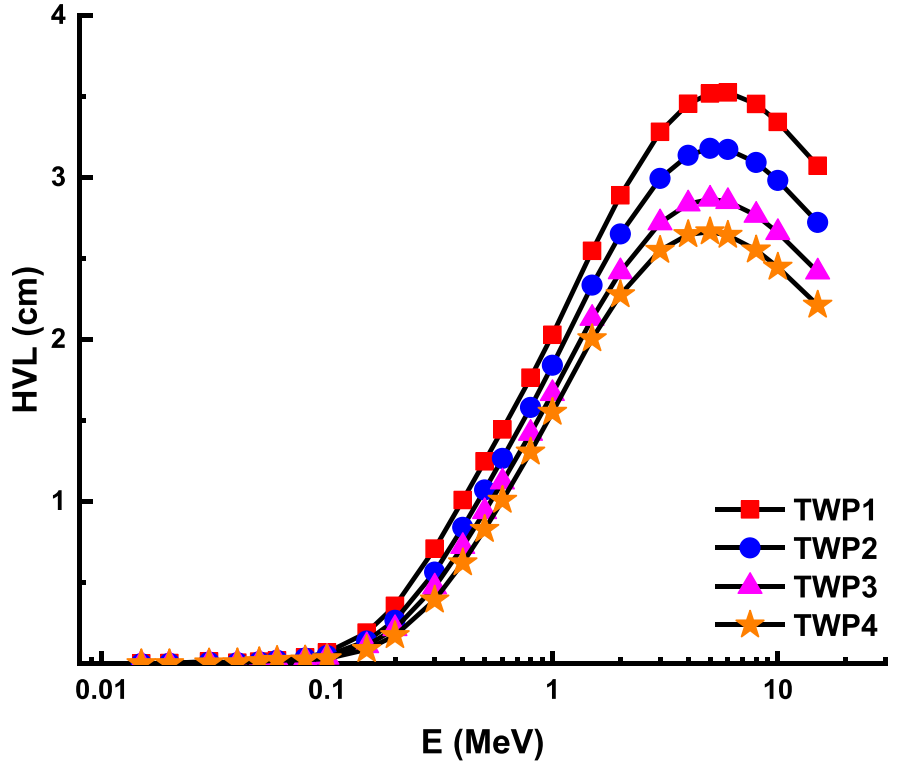

Fig. 6. Variations of half-value layer (HVL) with photon energy for all glasses.

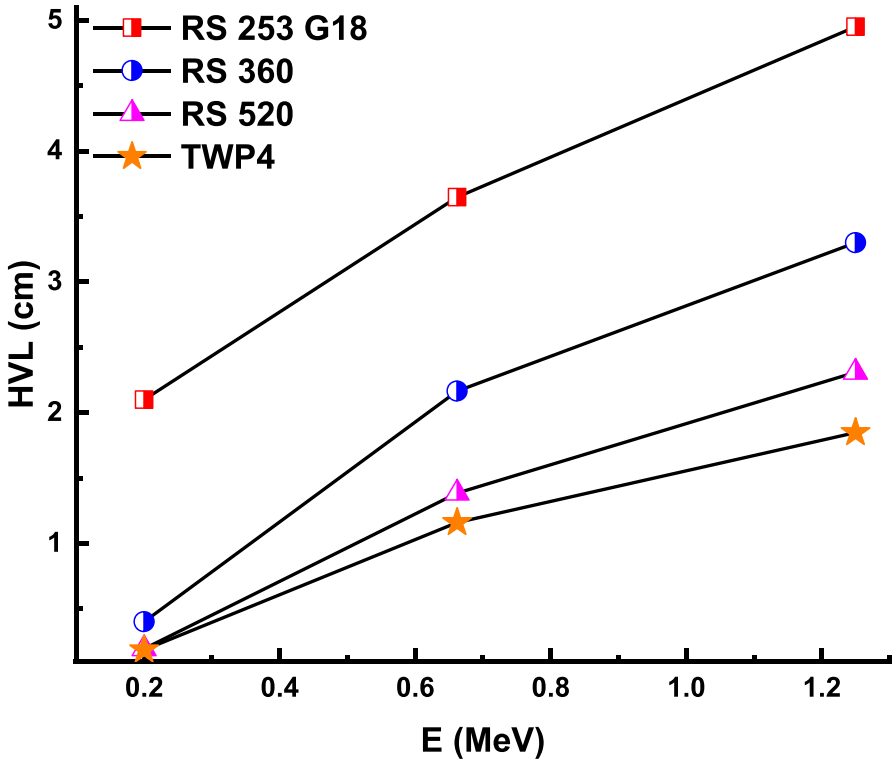

Fig. 7. Comparison of HVL of the TWP4 glass with some commercial glasses.

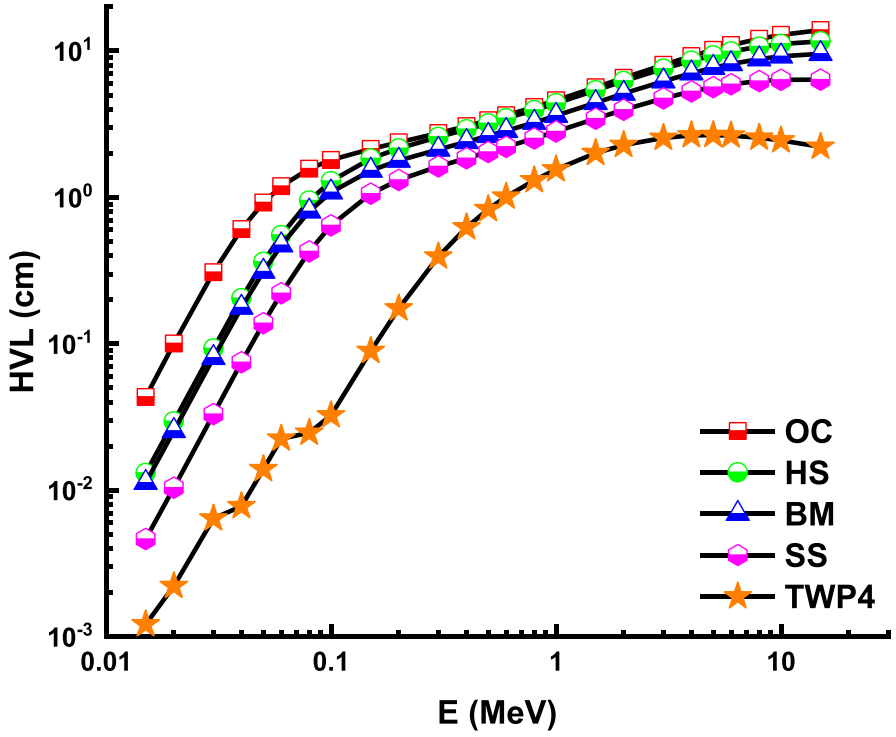

Fig. 8. Comparison of HVL of the TWP4 glass with some standard shielding concretes.

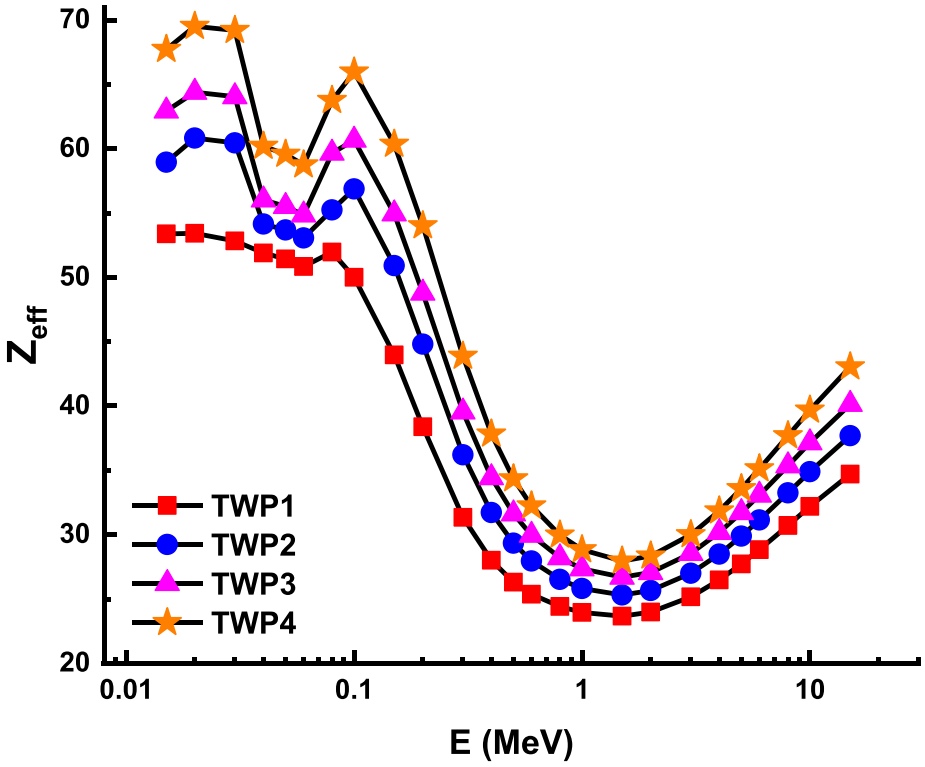

Fig. 9. Variation of effective atomic number (Z_{eff}) with photon energy for all glasses.

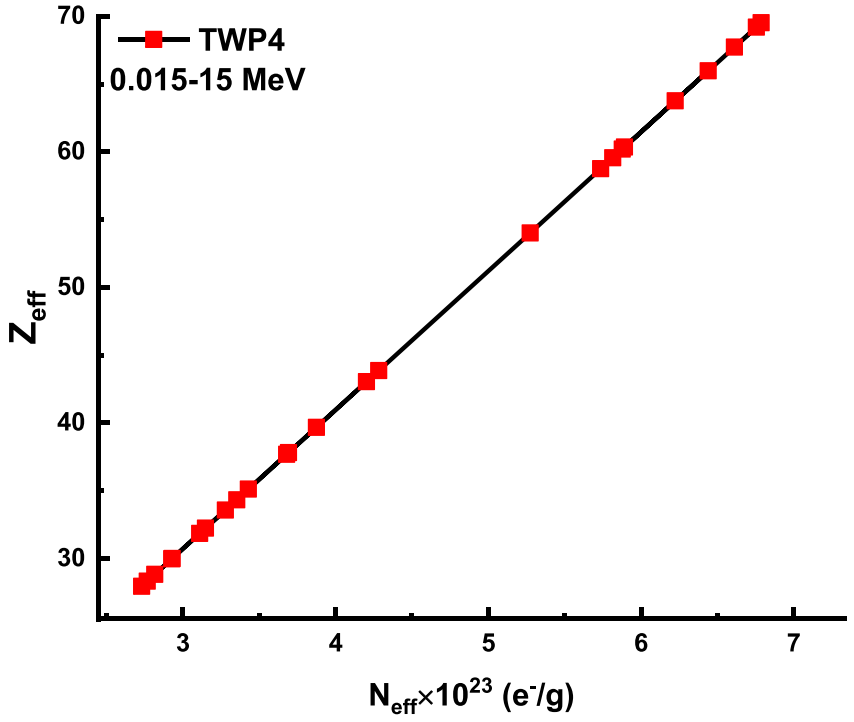

Fig. 10. Variation of effective atomic number (Z_{eff}) with effective electron density (N_{eff}) for TWP4 glass.

Table 4
Effective conductivity (C_{eff}) (S/m) for glass samples.

E (MeV)	TWP1	TWP2	TWP3	TWP4
1.50E−02	2.51E+09	2.80E+09	3.09E+09	3.35E+09
2.00E−02	2.51E+09	2.89E+09	3.16E+09	3.44E+09
3.00E−02	2.48E+09	2.87E+09	3.15E+09	3.42E+09
4.00E−02	2.44E+09	2.57E+09	2.75E+09	2.98E+09
5.00E−02	2.42E+09	2.55E+09	2.73E+09	2.95E+09
6.00E−02	2.39E+09	2.52E+09	2.70E+09	2.91E+09
8.00E−02	2.44E+09	2.63E+09	2.93E+09	3.15E+09
1.00E−01	2.35E+09	2.70E+09	2.98E+09	3.26E+09
1.50E−01	2.07E+09	2.42E+09	2.70E+09	2.99E+09
2.00E−01	1.80E+09	2.13E+09	2.40E+09	2.67E+09
3.00E−01	1.47E+09	1.72E+09	1.94E+09	2.17E+09
4.00E−01	1.32E+09	1.51E+09	1.69E+09	1.87E+09
5.00E−01	1.24E+09	1.39E+09	1.55E+09	1.70E+09
6.00E−01	1.19E+09	1.33E+09	1.47E+09	1.59E+09
8.00E−01	1.15E+09	1.26E+09	1.39E+09	1.48E+09
1.00E+00	1.13E+09	1.23E+09	1.34E+09	1.43E+09
1.50E+00	1.11E+09	1.20E+09	1.31E+09	1.38E+09
2.00E+00	1.13E+09	1.22E+09	1.33E+09	1.40E+09
3.00E+00	1.18E+09	1.28E+09	1.40E+09	1.48E+09
4.00E+00	1.24E+09	1.35E+09	1.48E+09	1.58E+09
5.00E+00	1.30E+09	1.42E+09	1.56E+09	1.66E+09
6.00E+00	1.35E+09	1.48E+09	1.63E+09	1.74E+09
8.00E+00	1.44E+09	1.58E+09	1.74E+09	1.86E+09
1.00E+01	1.51E+09	1.66E+09	1.82E+09	1.96E+09
1.50E+01	1.63E+09	1.79E+09	1.97E+09	2.13E+09

which indicates good mechanical strength of glass samples (Tables 7 and 8).

Conclusion

The influences of WO_3 and PbO on gamma shielding and mechanical properties of TeO_2-WO_3-PbO glasses are computed via different radiation attenuations factors via the XCOM database, FLUKA code, and Phy-X/PSD software. Moreover, the elastic parameters have been evaluated via both MMD and RD.

- It has been established that μ_m of glasses increases with the addition of WO_3 and PbO contents.
- The comparison of the MFP (ranged from 0.001752 to 3.193964) value of the TWP4 sample with other glasses shows that TWP4 exhibits better shielding ability.
- It was found that the TWP4 glass sample has a lower value of HVL (ranged from 0.18713 to 1.84819) than some commercial glasses and some concretes.
- Z_{eff}, N_{eff}, and C_{eff} values of the TWP4 sample have the largest value as compared to other investigated glasses.
- The EBF, EABF, Ψ_{proton}, Ψ_{Alpha}, and $\Psi_{Electron}$ value of the TWP4 sample has the lowest value as compared to other investigated glasses.
- σ value ranged from 0.24 to 0.26 that signifies the improvement in the cross-link density of glasses.

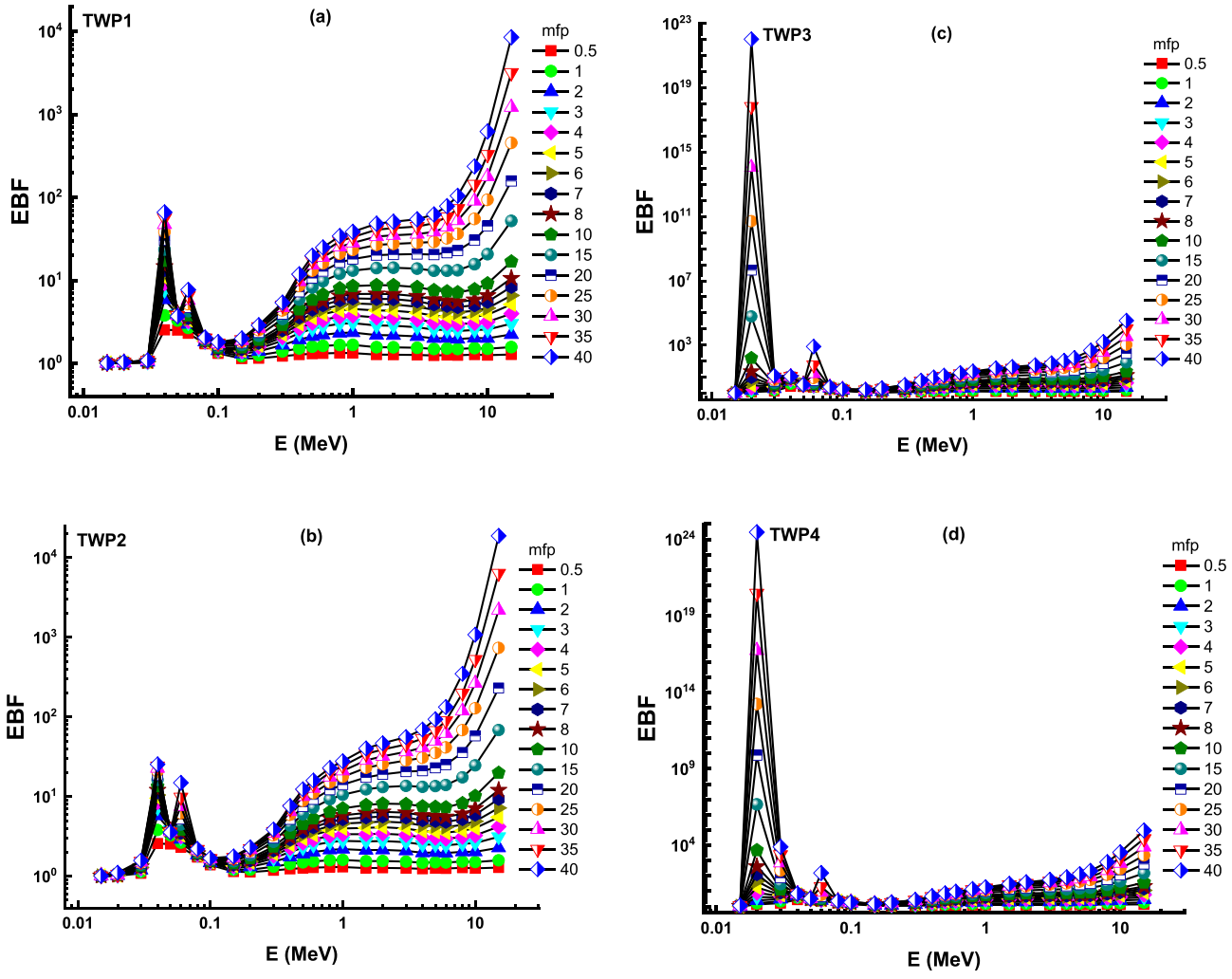

Fig. 11. (a-d) Variations of exposure buildup factor (EBF) with photon energy at different mean free paths for all glasses.

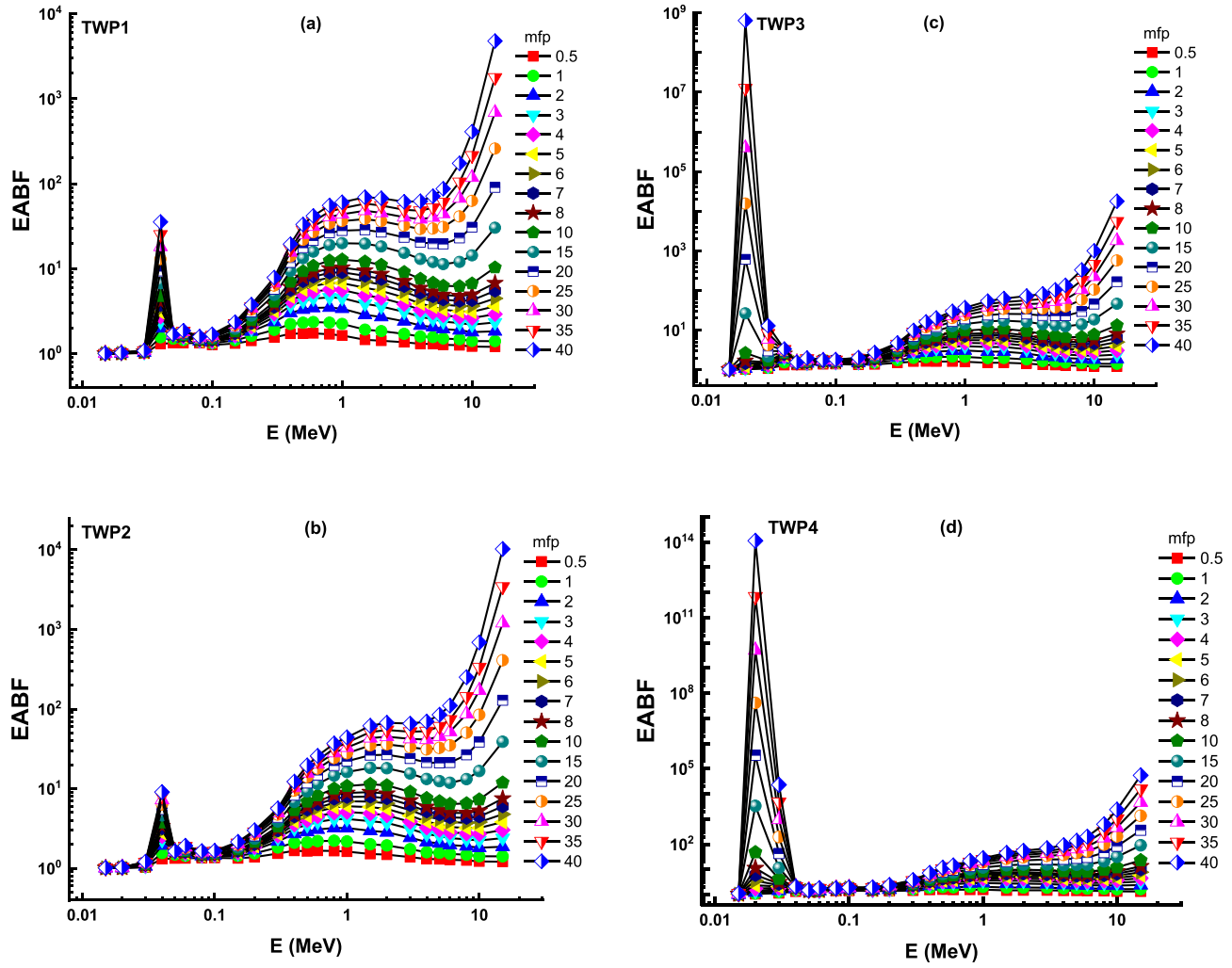

Fig. 12. (a-d) Variations of energy absorption buildup factor (EABF) with photon energy at different mean free paths for all glasses.

Table 5a
(EBF and EABF) G–P fitting coefficients (b, c, a, X_k and d) of **TWP1** glass sample.

E (MeV)	Z_{eq}	EBF					EABF				
		b	c	a	d	X_k	b	c	a	d	X_k
0.015	25.87	−0.5428	1.0041	1.5423	0.3481	5.6278	−0.5426	1.0041	1.5421	0.3477	5.6800
0.020	26.01	0.6204	1.0120	0.1299	−0.6174	11.3884	0.3193	1.0100	0.2579	−0.2956	18.2051
0.030	26.30	0.1916	1.0272	0.3724	−0.2888	27.4998	0.2515	1.0259	0.3235	−0.1898	18.0713
0.040	45.25	0.0919	3.7839	0.7068	−0.0719	24.6326	0.0989	1.5622	0.7228	−0.0368	18.9827
0.050	45.64	−0.0328	3.2890	0.2537	−0.0837	14.2642	0.0526	1.5049	0.2615	−0.0493	12.2896
0.060	45.90	0.5265	2.6817	0.1212	−0.1009	11.1378	0.3519	1.4499	0.1423	−0.0662	18.1011
0.080	49.28	0.8074	1.7958	0.0183	−0.1612	15.3631	0.7198	1.3853	0.0379	−0.2272	14.2234
0.100	49.62	0.6707	1.3856	0.0666	−0.3148	13.7883	0.6446	1.3308	0.0770	−0.3507	13.4265
0.150	50.10	0.2803	1.2186	0.3246	−0.1562	13.9467	0.4299	1.4379	0.1799	−0.2362	13.8582
0.200	50.38	0.1724	1.2571	0.4971	−0.0925	14.5959	0.3299	1.6179	0.2789	−0.1929	13.9154
0.300	50.71	0.1087	1.3946	0.6398	−0.0514	14.1880	0.2121	1.9054	0.4445	−0.1206	13.7899
0.400	50.89	0.0680	1.5155	0.7779	−0.0435	14.1373	0.1583	2.2358	0.5762	−0.1114	13.8687
0.500	51.02	0.0456	1.5913	0.8606	−0.0362	14.0661	0.1119	2.3237	0.6923	−0.0870	13.8715
0.600	51.09	0.0268	1.6267	0.9234	−0.0258	13.9853	0.0868	2.3612	0.7605	−0.0732	13.7267
0.800	51.17	0.0106	1.6662	0.9875	−0.0192	14.0141	0.0571	2.3238	0.8511	−0.0565	13.6265
1.000	51.21	0.0034	1.6699	1.0190	−0.0173	13.3954	0.0418	2.2433	0.9007	−0.0481	13.5055
1.500	50.47	−0.0201	1.5677	1.1184	−0.0049	14.2529	0.0064	1.9234	1.0270	−0.0258	13.6514
2.000	48.46	−0.0169	1.5641	1.1114	−0.0081	13.0139	0.0160	1.8492	1.0029	−0.0360	13.1110
3.000	45.59	0.0019	1.5410	1.0617	−0.0306	12.9106	0.0401	1.7167	0.9409	−0.0635	13.2382
4.000	44.35	0.0160	1.4941	1.0268	−0.0435	13.3819	0.0568	1.5953	0.9013	−0.0784	13.5575
5.000	43.69	0.0460	1.5124	0.9454	−0.0708	13.6126	0.0858	1.5673	0.8312	−0.1048	13.8049
6.000	43.29	0.0573	1.4939	0.9231	−0.0804	13.8374	0.0981	1.5138	0.8084	−0.1156	14.0174
8.000	42.77	0.0796	1.5304	0.8816	−0.0985	14.1510	0.1111	1.4797	0.7939	−0.1251	14.2952
10.000	42.48	0.0583	1.5021	0.9695	−0.0779	14.2080	0.0869	1.4133	0.8804	−0.1015	14.3461
15.000	42.33	0.0346	1.5738	1.1220	−0.0598	14.1489	0.0628	1.4063	1.0209	−0.0850	14.2715

Table 5b
(EBF and EABF) G–P fitting coefficients (b, c, a, X_k and d) of **TWP2** glass sample.

E (MeV)	Z_{eq}	EBF					EABF				
		b	c	a	d	X_k	b	c	a	d	X_k
0.015	27.84	−0.4016	1.0021	1.8627	0.2896	9.0673	−0.4016	1.0021	1.8627	0.2896	9.0673
0.020	29.05	0.7603	1.0167	0.1126	−1.0561	10.7925	0.4399	1.0071	0.2390	−0.5074	12.6375
0.030	29.47	0.2008	1.1334	0.3907	−0.0582	12.8713	0.2409	1.0385	0.4016	−0.1746	11.9846
0.040	44.74	0.0913	3.8082	0.6474	−0.0658	24.4378	0.1001	1.5509	0.6606	−0.0381	19.6366
0.050	45.09	−0.0741	3.2628	0.2223	−0.0634	13.9291	0.0226	1.4872	0.2310	−0.0244	11.7093
0.060	45.34	0.6063	2.6438	0.1050	−0.1074	12.0217	0.4139	1.4328	0.1258	−0.0835	17.6592
0.080	50.26	0.7734	1.8176	0.0248	−0.1438	15.4874	0.7013	1.4014	0.0412	−0.2154	14.2348
0.100	54.53	0.6701	1.4450	0.0447	−0.2190	14.2335	0.6464	1.4138	0.0518	−0.2312	13.9858
0.150	55.30	0.3420	1.1998	0.2569	−0.1944	13.7887	0.5210	1.4311	0.1257	−0.2763	13.7755
0.200	55.73	0.1909	1.2055	0.4586	−0.1022	14.2721	0.3823	1.5362	0.2242	−0.2204	13.8537
0.300	56.27	0.1286	1.3175	0.5866	−0.0611	13.8782	0.2645	1.8196	0.3595	−0.1512	13.5674
0.400	56.59	0.0858	1.4224	0.7172	−0.0501	14.1211	0.1964	2.0900	0.4927	−0.1314	13.8606
0.500	56.80	0.0595	1.4912	0.8048	−0.0398	14.0989	0.1381	2.1090	0.6194	−0.0986	13.8797
0.600	56.94	0.0409	1.5349	0.8656	−0.0304	13.8117	0.1108	2.1867	0.6877	−0.0841	13.7102
0.800	57.09	0.0232	1.5869	0.9331	−0.0235	13.6604	0.0763	2.2089	0.7850	−0.0651	13.6099
1.000	57.16	0.0142	1.6002	0.9729	−0.0222	13.2469	0.0595	2.1704	0.8393	−0.0571	13.5295
1.500	56.34	−0.0101	1.5408	1.0764	−0.0102	13.6986	0.0350	1.9990	0.9329	−0.0475	13.5507
2.000	54.21	−0.0049	1.5542	1.0686	−0.0172	13.0877	0.0406	1.9340	0.9271	−0.0559	13.2433
3.000	50.61	0.0054	1.5249	1.0534	−0.0342	13.0272	0.0512	1.7313	0.9127	−0.0745	13.2905
4.000	48.84	0.0160	1.4747	1.0334	−0.0446	13.4206	0.0618	1.5870	0.8930	−0.0845	13.6238
5.000	47.86	0.0460	1.4973	0.9532	−0.0722	13.6649	0.0900	1.5610	0.8270	−0.1104	13.8624
6.000	47.30	0.0584	1.4847	0.9292	−0.0827	13.8881	0.1042	1.5133	0.8008	−0.1230	14.0681
8.000	46.60	0.0776	1.5274	0.8989	−0.0984	14.1560	0.1116	1.4782	0.8027	−0.1275	14.3198
10.000	46.24	0.0529	1.5031	1.0025	−0.0743	14.1935	0.0859	1.4158	0.8978	−0.1030	14.3169
15.000	45.94	0.0304	1.5828	1.1638	−0.0582	14.0315	0.0609	1.4096	1.0509	−0.0867	14.1823

Table 5c
(EBF and EABF) G–P fitting coefficients (b, c, a, X_k and d) of **TWP3** glass sample.

E (MeV)	Z_{eq}	EBF					EABF				
		b	c	a	d	X_k	b	c	a	d	X_k
0.015	29.78	−0.2717	1.0016	1.9235	0.2260	11.2556	−0.2734	1.0016	1.9246	0.2278	11.3806
0.020	30.99	0.6311	1.2865	0.4482	−0.8731	11.2321	0.3663	1.0456	0.5556	−0.4199	13.6021
0.030	31.40	0.1844	1.5829	0.5164	−0.0868	16.3235	0.2167	1.1237	0.5267	−0.1646	14.8558
0.040	43.76	0.0901	3.8548	0.5332	−0.0540	24.0631	0.1025	1.5292	0.5411	−0.0404	20.8939
0.050	44.09	−0.1509	3.2142	0.1641	−0.0257	13.3069	−0.0332	1.4542	0.1744	0.0218	10.6321
0.060	44.33	0.7522	2.5746	0.0753	−0.1193	13.6363	0.5270	1.4018	0.0956	−0.1151	16.8519
0.080	53.65	0.3085	1.9370	0.1218	−0.0350	15.9498	0.3090	1.5053	0.1297	−0.0701	14.1701
0.100	57.72	0.5885	1.4860	0.0609	−0.1417	14.9886	0.5698	1.4736	0.0641	−0.1419	14.7229
0.150	58.52	0.3864	1.1949	0.2163	−0.2184	13.7604	0.5783	1.4376	0.0979	−0.2940	13.8113
0.200	58.97	0.2050	1.1837	0.4321	−0.1095	14.1941	0.4210	1.5083	0.1920	−0.2384	13.8165
0.300	59.53	0.1355	1.2799	0.5665	−0.0637	13.8287	0.2879	1.7520	0.3257	−0.1639	13.4800
0.400	59.86	0.0921	1.3758	0.6944	−0.0517	14.1665	0.2163	1.9950	0.4549	−0.1425	13.8262
0.500	60.08	0.0673	1.4453	0.7762	−0.0421	14.1227	0.1608	2.0656	0.5688	−0.1115	13.8664
0.600	60.21	0.0491	1.4904	0.8342	−0.0330	13.7816	0.1233	2.0860	0.6524	−0.0893	13.6863
0.800	60.38	0.0305	1.5472	0.9031	−0.0256	13.6749	0.0879	2.1368	0.7487	−0.0703	13.6050
1.000	60.44	0.0186	1.5640	0.9512	−0.0222	13.3818	0.0696	2.1193	0.8060	−0.0620	13.5199
1.500	59.71	−0.0042	1.5208	1.0524	−0.0135	13.7883	0.0412	1.9653	0.9102	−0.0508	13.5961
2.000	57.65	0.0019	1.5474	1.0438	−0.0222	13.0869	0.0546	1.9769	0.8839	−0.0671	13.3249
3.000	54.06	0.0129	1.5349	1.0288	−0.0400	13.2281	0.0738	1.8302	0.8520	−0.0945	13.4009
4.000	52.12	0.0226	1.4868	1.0144	−0.0500	13.5281	0.0782	1.6515	0.8521	−0.0994	13.7065
5.000	51.02	0.0497	1.5087	0.9463	−0.0754	13.7317	0.1002	1.6039	0.8057	−0.1203	13.9240
6.000	50.38	0.0600	1.4888	0.9302	−0.0846	13.9355	0.1101	1.5308	0.7911	−0.1294	14.1098
8.000	49.59	0.0762	1.5253	0.9114	−0.0983	14.1595	0.1120	1.4771	0.8092	−0.1292	14.3377
10.000	49.16	0.0491	1.5038	1.0264	−0.0717	14.1829	0.0852	1.4175	0.9105	−0.1040	14.2958
15.000	48.78	0.0273	1.5893	1.1944	−0.0571	13.9453	0.0596	1.4120	1.0730	−0.0879	14.1168

Finally, the results after evaluating the MAC, LAC, MFP, HVL, Z_{eff}, N_{eff}, ECS, ACS, EBF, EABF, Σ_R, Ψ_{proton}, Ψ_{Alpha}, and $\Psi_{Electron}$ values observed that glass sample TWP4 has a better shielding ability and it may be used in some nuclear radiation shielding applications in future.

CRediT authorship contribution statement

A.M.A. Mostafa: Conceptualization, Methodology, Writing - original draft. **Shams A.M. Issa:** Conceptualization, Writing - original draft, Investigation, Supervision. **Hesham M.H. Zakaly:** Writing - original draft, Investigation, Methodology. **M.H.M. Zaid:** Funding acquisition, Supervision. **H.O. Tekin:** Investigation, Conceptualization, Supervision. **K.A. Matori:** Funding acquisition, Supervision. **H.A.A. Sidek:** Funding acquisition, Supervision. **Reda Elsaman:** Conceptualization, Investigation.

Declaration of Competing Interest

The authors declare that they have no known competing financial interests or personal relationships that could have appeared to influence the work reported in this paper.

Table 5d
(EBF and EABF) G–P fitting coefficients (b, c, a, X_k and d) of **TWP4** glass sample.

E (MeV)	Z_{eq}	EBF					EABF				
		b	c	a	d	X_k	b	c	a	d	X_k
0.015	31.87	−0.1743	1.0030	1.6169	0.1601	11.5241	−0.1802	1.0030	1.6207	0.1667	11.9670
0.020	33.89	0.4521	1.6601	0.9128	−0.6198	11.8406	0.2644	1.0990	0.9939	−0.2987	14.9375
0.030	34.27	0.1617	2.2017	0.6894	−0.1261	21.0769	0.1835	1.2410	0.6990	−0.1510	18.8091
0.040	42.39	0.0885	3.9215	0.3698	−0.0370	23.5267	0.1060	1.4981	0.3700	−0.0438	22.6942
0.050	42.69	−0.2610	3.1444	0.0805	0.0283	12.4137	−0.1133	1.4070	0.0932	0.0881	9.0855
0.060	42.94	0.9595	2.4762	0.0332	−0.1362	15.9310	0.6877	1.3576	0.0527	−0.1599	15.7045
0.080	55.23	0.1009	1.9903	0.1651	0.0136	16.1563	0.1338	1.5517	0.1692	−0.0053	14.1413
0.100	62.31	0.1474	1.5830	0.1943	0.0083	18.2043	0.1426	1.5991	0.1922	0.0044	17.4169
0.150	63.21	0.4610	1.1976	0.1583	−0.2544	13.8203	0.6641	1.4629	0.0653	−0.3099	13.9910
0.200	63.69	0.2276	1.1605	0.3915	−0.1211	14.1808	0.4822	1.4864	0.1468	−0.2654	13.7633
0.300	64.30	0.1438	1.2310	0.5422	−0.0664	13.8039	0.3186	1.6539	0.2843	−0.1800	13.3778
0.400	64.64	0.1006	1.3150	0.6643	−0.0542	14.2238	0.2437	1.8653	0.4052	−0.1578	13.7752
0.500	64.87	0.0780	1.3846	0.7373	−0.0455	14.1481	0.1915	2.0008	0.5024	−0.1289	13.8398
0.600	65.02	0.0604	1.4307	0.7915	−0.0368	13.7435	0.1402	1.9476	0.6056	−0.0962	13.6513
0.800	65.19	0.0404	1.4927	0.8624	−0.0286	13.6925	0.1036	2.0329	0.7003	−0.0769	13.5975
1.000	65.25	0.0255	1.5148	0.9188	−0.0230	13.4959	0.0833	2.0409	0.7613	−0.0681	13.5127
1.500	64.61	0.0036	1.4902	1.0200	−0.0178	14.0288	0.0468	1.8953	0.8878	−0.0524	13.6910
2.000	62.68	0.0012	1.5063	1.0424	−0.0198	13.1374	0.0589	1.9026	0.8688	−0.0689	13.3610
3.000	58.89	0.0187	1.5275	1.0104	−0.0444	13.3533	0.0923	1.8747	0.8024	−0.1108	13.5013
4.000	56.71	0.0362	1.5210	0.9725	−0.0603	13.7280	0.1091	1.7869	0.7728	−0.1268	13.8419
5.000	55.40	0.0648	1.5847	0.9030	−0.0857	13.9013	0.1335	1.7905	0.7272	−0.1495	14.0622
6.000	54.62	0.0705	1.5944	0.8999	−0.0894	14.1022	0.1330	1.7222	0.7380	−0.1477	14.2147
8.000	53.67	0.0744	1.6992	0.9217	−0.0941	14.1708	0.1212	1.7090	0.7922	−0.1378	14.3075
10.000	53.15	0.0419	1.6973	1.0629	−0.0650	14.1240	0.0859	1.6369	0.9215	−0.1071	14.1826
15.000	52.67	0.0189	1.8252	1.2502	−0.0499	13.8188	0.0554	1.6406	1.1094	−0.0870	13.9631

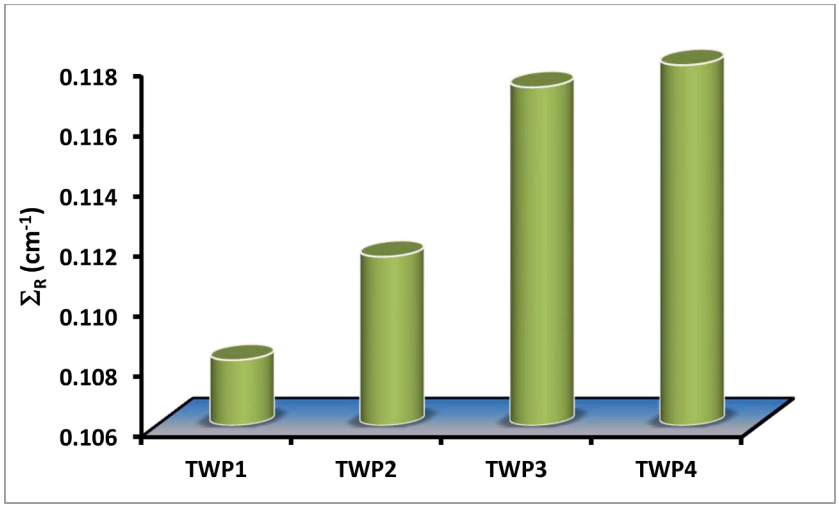

Fig. 13. Effective removal cross-sections for fast neutrons (Σ_R), for all glasses.

Table 6
Comparison of Σ_R of glass TWP4 with reported different nuclear radiation shielding substances.

Sample	Σ_R	Reference
TWP4	**0.1185**	**This work**
Graphite	0.0771	[42]
Water	0.1024	
Ordinary concrete	0.0937	[40]
Hematite-serpentine concrete	0.0967	
Ilmenite-limonite concrete	0.0950	
Basalt-magnetite concrete	0.1102	
Ilmenite concrete	0.1121	
VPZn8 glass	0.092274	[43]
C20 glass	0.106586	[44]
TBBT30 glass	0.1169	[45]
S2 ceramic	0.0695	[46]
95TeLi glass	0.105831	[47]
Polyamide polymer	0.1151	[48]

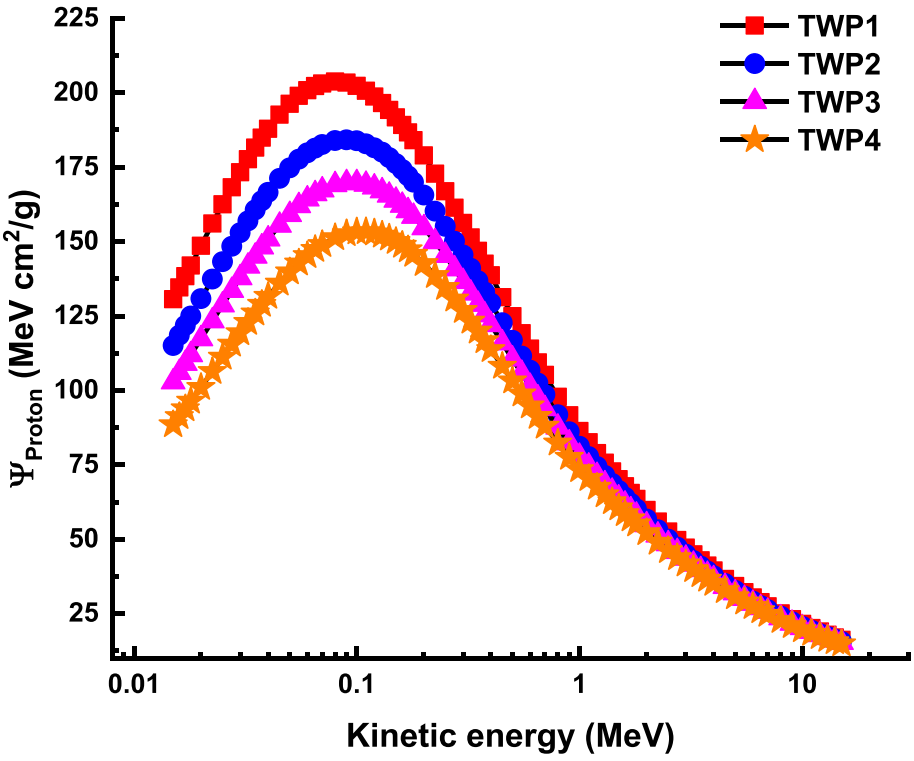

Fig. 14. Variations of proton mass stopping power (ψ_{Proton}) as a function of kinetic energy for all glasses.

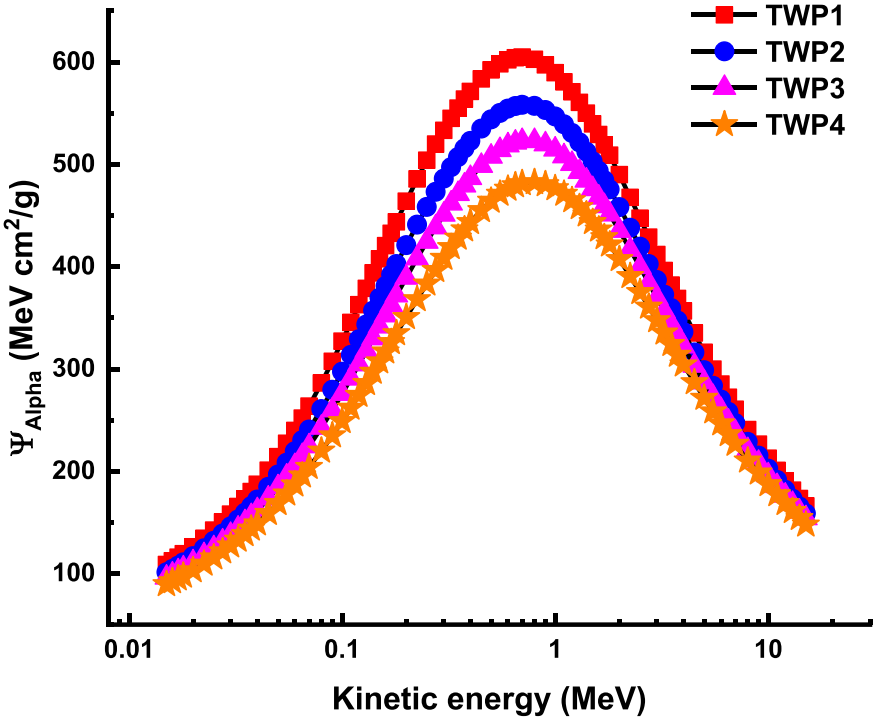

Fig. 15. Variations of alpha mass stopping power (ψ_{Alpha}) as a function of kinetic energy for all glasses.

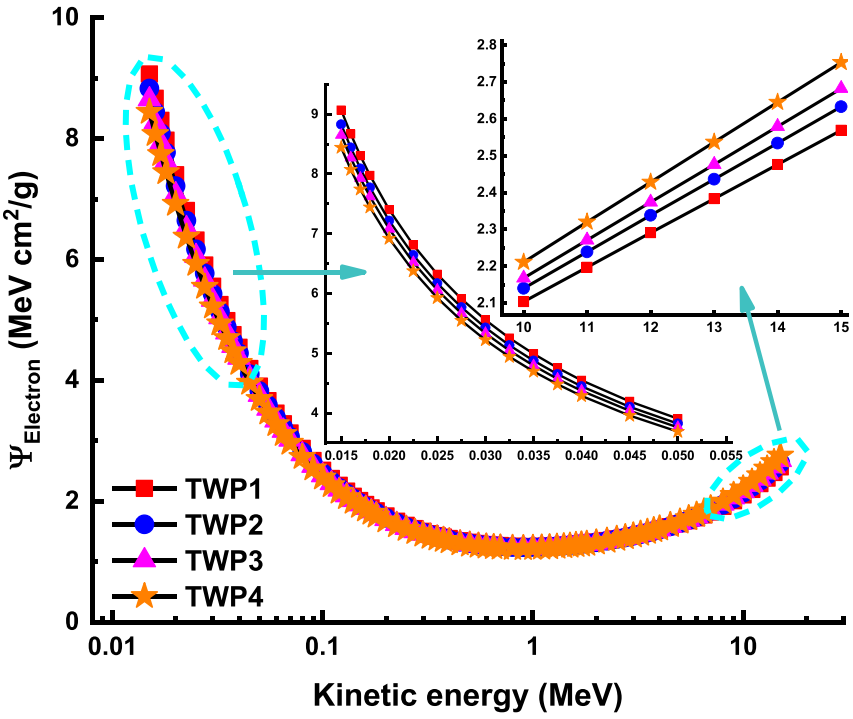

Fig. 16. Variations of electron mass stopping power ($\psi_{Electron}$) as a function of kinetic energy for all glasses.

Table 7
Mechanical properties according to Makishima and Mackenzie model (MMD).

Code	V_t	G_t	Y_{MM} (Gpa)	K_{MM} (Gpa)	G_{MM} (Gpa)	L_{MM} (Gpa)	σ
TWP1	0.53	13.25	59.13	37.76	25.48	71.73	0.24
TWP2	0.54	12.73	57.62	37.32	24.75	70.33	0.24
TWP3	0.57	12.54	59.34	40.19	25.25	73.86	0.25
TWP4	0.58	12.87	62.80	43.86	26.55	79.26	0.26

Table 8
Mechanical properties according to Rocherulle model (RD).

Code	C_t	Y_B (Gpa)	K_B (Gpa)	G_B (Gpa)	L_B (Gpa)
TWP1	0.58	64.12	44.40	27.16	80.62
TWP2	0.57	60.84	41.62	25.83	76.06
TWP3	0.57	59.72	40.70	25.38	74.54
TWP4	0.57	61.84	42.53	26.23	77.50

References

[1] Yim M-S, Ocken H. Radiation dose management in nuclear power plants. Prog Nucl Energy 2001;39:31–51. https://doi.org/10.1016/S0149-1970(01)00002-6.

[2] Donya M, Radford M, ElGuindy A, Firmin D, Yacoub MH. Radiation in medicine: Origins, risks and aspirations. Global Cardiology Sci Practice 2014;2014:57. https://doi.org/10.5339/gcsp.2014.57.

[3] Landgraf M, Gaularte L, Martins C, Cestari A, Nunes T, Aragon L, et al. Use of irradiation to improve the microbiological safety of minimally processed fruits and vegetables. IAEA-TECDOC 2006;1530:41–59.

[4] Guo-hui W, Man-li He, Fan-chao C, Jun-dong F, Yao-dong D. Enhancement of flame retardancy and radiation shielding properties of ethylene vinyl acetate based radiation shielding composites by EB irradiation. Prog Nucl Energy 2019;112: 225–32. https://doi.org/10.1016/j.pnucene.2019.01.001.

[5] Clegg FM, Sears M, Friesen M, Scarato T, Metzinger R, Russell C, et al. Building science and radiofrequency radiation: What makes smart and healthy buildings. Build Environ 2020;176:106324. https://doi.org/10.1016/j.buildenv.2019.106324.

[6] Elazaka AI, Zakaly HMH, Issa SAM, Rashad M, Tekin HO, Saudi HA, et al. New approach to removal of hazardous Bypass Cement Dust (BCD) from the environment: 20Na_2O-20$BaCl_2$-(60-x)B_2O_3-(x)BCD glass system and Optical, mechanical, structural and nuclear radiation shielding competences. J Hazard Mater 2021;403:123738. https://doi.org/10.1016/j.jhazmat.2020.123738.

[7] Levitt BB, Lai H. Biological effects from exposure to electromagnetic radiation emitted by cell tower base stations and other antenna arrays. Environ Rev 2010;18: 369–95. https://doi.org/10.1139/A10-018.

[8] Karinen A, Heinavaara S, Nylund R, Leszczynski D. Mobile phone radiation might alter protein expression in human skin. BMC Genomics 2008;9(1):77. https://doi.org/10.1186/1471-2164-9-77.

[9] Abouhaswa AS, Zakaly HMH, Issa SAM, Pyshkina M, El-Mallawany R, Mostafa MYA. Lead borate glasses and synergistic impact of lanthanum oxide additive: optical and nuclear radiation shielding behaviors. J Mater Sci: Mater Electron 2020. https://doi.org/10.1007/s10854-020-04009-y.

[10] Rammah YS, Sayyed MI, Ali AA, Tekin HO, El-Mallawany R. Optical properties and gamma-shielding features of bismuth borate glasses. Appl Phys A 2018;124:832. https://doi.org/10.1007/s00339-018-2252-7.

[11] Ali AA, Rammah YS, El-Mallawany R, Souri D. FTIR and UV spectra of pentaternary borate glasses. Measurement 2017;105:72–7. https://doi.org/10.1016/j.measurement.2017.04.010.

[12] Lotfi-Omran O, Sadrmomtazi A, Nikbin IM. A comprehensive study on the effect of water to cement ratio on the mechanical and radiation shielding properties of heavyweight concrete. Constr Build Mater 2019;229:116905. https://doi.org/10.1016/j.conbuildmat.2019.116905.

[13] Papachristoforou M, Papayianni I. Radiation shielding and mechanical properties of steel fiber reinforced concrete (SFRC) produced with EAF slag aggregates. Radiat Phys Chem 2018;149:26–32. https://doi.org/10.1016/j.radphyschem.2018.03.010.

[14] Dong MG, El-Mallawany R, Sayyed MI, Tekin HO. Shielding properties of 80TeO_2–5TiO_2–(15−x) WO_3–xAnOm glasses using WinXCom and MCNP5 code. Radiat Phys Chem 2017;141:172–8.

[15] Tekin HO, Kassab LRP, Kilicoglu O, Magalhães ES, Issa SAM, da Silva Mattos GR. Newly developed tellurium oxide glasses for nuclear shielding applications: An extended investigation. J Non-Cryst Solids 2020;528:119763. https://doi.org/10.1016/j.jnoncrysol.2019.119763.

[16] Al-Buriahi MS, Rashad M, Alalawi A, Sayyed MI. Effect of Bi_2O_3 on mechanical features and radiation shielding properties of boro-tellurite glass system. Ceram Int 2020;46:16452–8. https://doi.org/10.1016/j.ceramint.2020.03.208.

[17] Ali AA, Shaaban MH. Optical and electrical properties of Nd^{3+} Doped TeBiY borate glasses. Silicon 2018;10:1503–11. https://doi.org/10.1007/s12633-017-9633-y.

[18] Gaikwad DK, Sayyed MI, Obaid SS, Issa SAM, Pawar PP. Gamma ray shielding properties of TeO_2-ZnF_2-As_2O_3-Sm_2O_3 glasses. J Alloy Compd 2018;765:451–8. https://doi.org/10.1016/j.jallcom.2018.06.240.

[19] Kumar A. Gamma ray shielding properties of PbO-Li 2 O-B 2 O 3 glasses. Radiat Phys Chem 2017;136:50–3.

[20] Upender G, Chandra Mouli V. Optical, thermal and electrical properties of ternary TeO_2–WO_3–PbO glasses. J Mol Struct 2011;1006(1-3):159–65. https://doi.org/10.1016/j.molstruc.2011.09.001.

[21] Takaishi T, Takahashi M, Jin J, Uchino T, Yoko T, Takahashi M. Structural study on PbO-SiO_2 glasses by X-ray and neutron diffraction and 29Si MAS NMR measurements. J Am Ceramic Soc 2005;88:1591–6. https://doi.org/10.1111/j.1551-2916.2005.00297.x.

[22] Al-Hadeethi Y, Sayyed MI. The influence of PbO on the radiation attenuation features of tellurite glass. Ceram Int 2019;45:24230–5. https://doi.org/10.1016/j.ceramint.2019.08.133.

[23] Alalawi A, Al-Buriahi MS, Sayyed MI, Akyildirim H, Arslan H, Zaid MHM, et al. Influence of lead and zinc oxides on the radiation shielding properties of tellurite glass systems. Ceram Int 2020;46:17300–6. https://doi.org/10.1016/j.ceramint.2020.04.017.

[24] Lambson EF, Saunders GA, Bridge B, El-Mallawany RA. The elastic behaviour of TeO_2 glass under uniaxial and hydrostatic pressure. J Non-Cryst Solids 1984;69:117–33. https://doi.org/10.1016/0022-3093(84)90128-5.

[25] Berzelius J. Tellurite glasses. Ann Phys Chemie 1834.

[26] Stanworth JE. Tellurite Glasses. Nature 1952;169:581–2. https://doi.org/10.1038/169581b0.

[27] Stanworth J. J Soc Glas Tech 1954;38:581–2.

[28] Told F. Systematic analysis of optical glasses concerning their refractive indices and densities. Glas Berichte 1960.

[29] Prod'homme L. A new approach to the thermal change in the refractive index of glasses. Phys Chem Glas 1960;1:119–22.

[30] Ritland HN. Relation between refractive index and density of a glass at constant temperature. J American Ceramic Society 1955;38:86–8. https://doi.org/10.1111/j.1151-2916.1955.tb14581.x.

[31] El-Mallawany Raouf. The optical properties of tellurite glasses. J Appl Phys 1992;72(5):1774–7. https://doi.org/10.1063/1.351649.

[32] Munoz-Martín D, Villegas MA, Gonzalo J, Fernández-Navarro JM. Characterisation of glasses in the TeO_2–WO_3–PbO system. J Eur Ceram Soc 2009;29(14):2903–13. https://doi.org/10.1016/j.jeurceramsoc.2009.04.018.

[33] Akçalı Ö, Çağlar M, Toker O, Bilmez B, Kavanoz HB, İçelli O. An investigation on gamma-ray shielding properties of quaternary glassy composite ($Na_2Si_3O_7$/Bi_2O_3/B_2O_3/Sb_2O_3) by BXCOM and MCNP 6.2 code. Prog Nucl Energy 2020;125:103364. https://doi.org/10.1016/j.pnucene.2020.103364.

[34] Tekin HO, Issa SAM, Kavaz E, Altunsoy Guclu EE. The direct effect of Er2O3 on bismuth barium telluro borate glasses for nuclear security applications. Mater Res Express 2019;6. https://doi.org/10.1088/2053-1591/ab4cb5. 115212.

[35] Issa SAM, Sayyed MI, Kurudirek M. Study of gamma radiation shielding properties of ZnO-TeO_2 glasses. Bull Mater Sci 2017;40:841–57.

[36] Aşkın A. Evaluation of the radiation shielding capabilities of the $Na_2B_4O_7$–SiO_2–MoO_3-Dy_2O_3 glass quaternary using Geant4 simulation code and Phy-X/PSD database. Ceram Int 2020;46:9096–102. https://doi.org/10.1016/j.ceramint.2019.12.158.

[37] Lakshminarayana G, Elmahroug Y, Kumar A, Dong MG, Lee D-E, Yoon J, et al. TeO_2–B_2O_3–ZnO–La_2O_3 glasses: γ-ray and neutron attenuation characteristics analysis by WinXCOM program, MCNP5, Geant4, and Penelope simulation codes. Ceram Int 2020;46:16620–35. https://doi.org/10.1016/j.ceramint.2020.03.235.

[38] Bagheri R, Adeli R. Gamma-ray shielding properties of phosphate glasses containing Bi_2O_3, PbO, and BaO in different rates. Radiat Phys Chem 2020;174:108918. https://doi.org/10.1016/j.radphyschem.2020.108918.

[39] Issa SAM, Ali AM, Susoy G, Tekin HO, Saddeek YB, Elsaman R, et al. Mechanical, physical and gamma ray shielding properties of xPbO-(50–x) MoO_3–$50V_2O_5$ ($25 \leq x \leq 45$ mol %) glass system. Ceram Int 2020;46:20251–63. https://doi.org/10.1016/j.ceramint.2020.05.107.

[40] Al-Buriahi MS, Mann KS. Radiation shielding investigations for selected tellurite-based glasses belonging to the TNW system. Mater Res Express 2019;6. https://doi.org/10.1088/2053-1591/ab3f85. 105206.

[41] Issa SAM, Hamdalla TA, Darwish AAA. Effect of ErCl 3 in gamma and neutron parameters for different concentration of ErCl 3 -SiO 2 (EDFA) for the signal protection from nuclear radiation. J Alloy Compd 2017;698:234–40. https://doi.org/10.1016/j.jallcom.2016.12.176.

[42] Issa S, Sayyed M, Kurudirek M. Investigation of gamma radiation shielding properties of some zinc tellurite glasses. J Phys Sci 2016;27:97–119.

[43] Issa SAM, Mostafa AMA, Hanafy TA, Dong M, Xue X. Comparison study of photon attenuation characteristics of Poly vinyl alcohol (PVA) doped with $Pb(NO_3)_2$ by MCNP5 code, XCOM and experimental results. Prog Nucl Energy 2019;111:15–23. https://doi.org/10.1016/j.pnucene.2018.10.018.

[44] Berger MJ, Hubbell JH. XCOM: Photon Cross-Sections Database, Web Version 1.2 n.d.

[45] Şakar E, Özpolat ÖF, Alım B, Sayyed MI, Kurudirek M. Phy-X / PSD: Development of a user friendly online software for calculation of parameters relevant to radiation shielding and dosimetry. Radiat Phys Chem 2020;166:108496. https://doi.org/10.1016/j.radphyschem.2019.108496.

[46] Mostafa AMA, Zakaly HMH, Pyshkina M, Issa SAM, Tekin HO, Sidek HAA, et al. Multi-objective optimization strategies for radiation shielding performance of BZBB glasses using Bi_2O_3: A FLUKA Monte Carlo code calculations. J Mater Res Technol 2020;9(6):12335–45. https://doi.org/10.1016/j.jmrt.2020.08.077.

[47] Zakaly HM, Abouhaswa AS, Issa SAM, Mostafa MYA, Pyshkina M, El-Mallawany R. Optical and nuclear radiation shielding properties of zinc borate glasses doped with lanthanum oxide. J Non-Cryst Solids 2020;543:120151. https://doi.org/10.1016/j.jnoncrysol.2020.120151.

[48] Rashad M, Tekin HO, Zakaly HM, Pyshkina M, Issa SAM, Susoy G. Physical and nuclear shielding properties of newly synthesized magnesium oxide and zinc oxide nanoparticles. Nucl Eng Technol 2020;52:2078–84. https://doi.org/10.1016/j.net.2020.02.013.

[49] Ballarini F, Battistoni G, Brugger M, Campanella M, Carboni M, Cerutti F, et al. The physics of the FLUKA code: Recent developments. Adv Space Res 2007;40:1339–49. https://doi.org/10.1016/j.asr.2007.05.031.

[50] Battistoni G, Boehlen T, Cerutti F, Chin PW, Esposito LS, Fassò A, et al. Overview of the FLUKA code. Ann Nucl Energy 2015;82:10–8. https://doi.org/10.1016/j.anucene.2014.11.007.

[51] Ferrari A, Sala PR, Fasso A, Ranft J. FLUKA: A Multi-Particle Transport Code. CERN-2005-10 2005:INFN/TC 05/11, SLAC-R-773. https://doi.org/10.2172/877507.

[52] Wielopolski L, Song Z, Orion I, Hanson AL, Hendrey G. Basic considerations for Monte Carlo calculations in soil. Appl Radiat Isot 2005;62:97–107. https://doi.org/10.1016/j.apradiso.2004.06.003.

[53] Makishima A, Mackenzie JD. Direct calculation of Young's modulus of glass. J Non Cryst Solids 1973;12:35–45. https://doi.org/10.1016/0022-3093(73)90053-7.

[54] Makishima A, Mackenzie JD. Calculation of bulk modulus, shear modulus and Poisson's ratio of glass. J Non-Cryst Solids 1975;17:147–57. https://doi.org/10.1016/0022-3093(75)90047-2.

[55] Rocherulle J, Ecolivet C, Poulain M, Verdier P, Laurent Y. Elastic moduli of oxynitride glasses. J Non-Cryst Solids 1989;108:187–93. https://doi.org/10.1016/0022-3093(89)90582-6.

[56] https://www.schott.com/d/advanced_optics/352fbb5f-4d56-49d3-bb47-256437d58f0a/1.4/schott-radiation-shielding-glass-may-2013-eng.pdf. (Accessed July 2020). n.d.

[57] Bashter II. Calculation of radiation attenuation coefficients for shielding concretes. Ann Nucl Energy 1997;24:1389–401. https://doi.org/10.1016/S0306-4549(97)00003-0.

[58] Al-Hadeethi Y, Sayyed MI. Analysis of borosilicate glasses doped with heavy metal oxides for gamma radiation shielding application using Geant4 simulation code. Ceram Int 2019;45:24858–64. https://doi.org/10.1016/j.ceramint.2019.08.234.

[59] Al-Buriahi MS, Abouhaswa AS, Tekin HO, Sriwunkum C, El-Agawany FI, Nutaro T, et al. Structure, optical, gamma-ray and neutron shielding properties of NiO doped B_2O_3–$BaCO_3$–Li_2O_3 glass systems. Ceram Int 2020;46:1711–21. https://doi.org/10.1016/j.ceramint.2019.09.144.

[60] Kilic G, Ilik E, Mahmoud KA, El-Mallawany R, El-Agawany FI, Rammah YS. Novel zinc vanadyl boro-phosphate glasses: ZnO–V_2O_5– $_P2O5$–$_B2O3$: Physical, thermal, and nuclear radiation shielding properties. Ceram Int 2020;46:19318–27. https://doi.org/10.1016/j.ceramint.2020.04.272.

[61] Susoy G, Guclu EEA, Kilicoglu O, Kamislioglu M, Al-Buriahi MS, Abuzaid MM, et al. The impact of Cr_2O_3 additive on nuclear radiation shielding properties of LiF–SrO–B_2O_3 glass system. Mater Chem Phys 2020;242:122481. https://doi.org/10.1016/j.matchemphys.2019.122481.

[62] Rammah YS, Kavaz E, Akyildirim H, El-Agawany FI. Evaluation of photon, neutron, and charged particle shielding competences of TeO_2-B_2O_3-Bi_2O_3-TiO_2 glasses. J Non-Cryst Solids 2020;535:119960. https://doi.org/10.1016/j.jnoncrysol.2020.119960.

[63] Oto B, Kavaz E, Durak H, Aras A, Madak Z. Effect of addition of molybdenum on photon and fast neutron radiation shielding properties in ceramics. Ceram Int 2019;45:23681–9. https://doi.org/10.1016/j.ceramint.2019.08.082.

[64] Kamislioglu M, Altunsoy Guclu EE, Tekin HO. Comparative evaluation of nuclear radiation shielding properties of $xTeO_2$+ (100–x)Li_2O glass system. Appl Phys A 2020;126:95. https://doi.org/10.1007/s00339-020-3284-3.

[65] Kaçal MR, Akman F, Sayyed MI, Akman F. Evaluation of gamma-ray and neutron attenuation properties of some polymers. Nucl Eng Technol 2019;51:818–24. https://doi.org/10.1016/j.net.2018.11.011.

[66] Sayyed MI, Issa SAM, Tekin HO, Saddeek YB. Comparative study of gamma-ray shielding and elastic properties of BaO–Bi_2O_3–B_2O_3 and ZnO–Bi_2O_3–B_2O_3 glass systems. Mater Chem Phys 2018;217:11–22. https://doi.org/10.1016/j.matchemphys.2018.06.034.

[67] Issa SAM, Saddeek YB, Tekin HO, Sayyed MI, Shaaban KS. Investigations of radiation shielding using Monte Carlo method and elastic properties of PbO-SiO_2-B_2O_3-Na_2O glasses. Curr Appl Phys 2018;18:717–27. https://doi.org/10.1016/j.cap.2018.02.018.

[68] Saddeek YB. Structural and acoustical studies of lead sodium borate glasses. J Alloy Compd 2009;467:14–21. https://doi.org/10.1016/j.jallcom.2007.11.126.